Reductive Stress Selectively Disrupts Collagen Homeostasis and Modifies Growth Factor-independent Signaling Through the MAPK/Akt Pathway in Human Dermal Fibroblasts

Authors

Naomi A. Carne, Steven Bell, Adrian P. Brown, Arto Määttä, Michael J. Flagler, and Adam M. Benham

Correspondence

adam.benham@durham.ac.uk

In Brief

The skin fibroblast response to reductive stress has been characterized by label-free, data independent acquisition (DIA) proteomics, in the presence or absence of platelet-derived growth factor (PDGF). The fibroblast proteome is remarkably stable in the face of reductive stress, but some key proteins decline, including mitogen activated protein kinase (MAPK) pathway targets and a subset of extracellular matrix proteins. Signal transduction analysis reveals that reductants directly stimulate Akt phosphorylation and modulate MAPK phosphorylation.

Graphical Abstract

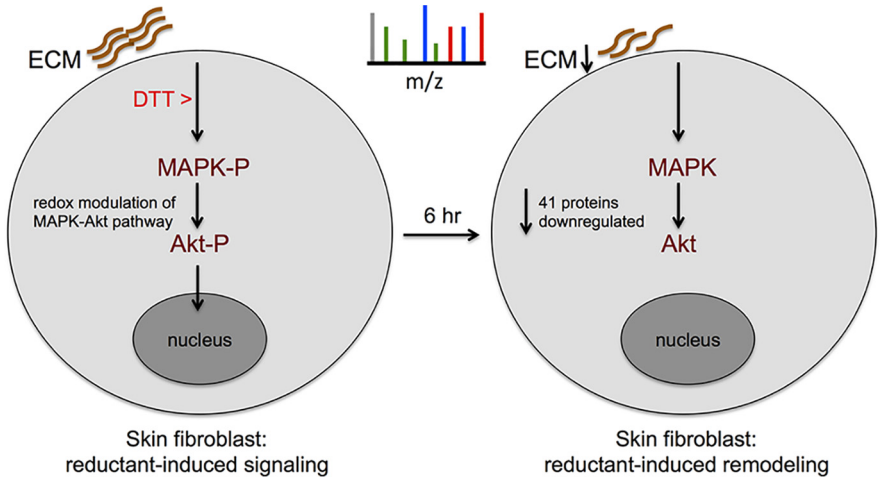

Highlights

- Changes to the proteome of skin fibroblasts subjected to reductive stress have been quantitated.
- Only a small set of proteins is selectively diminished upon exposure to reductants.
- Collagens (COL1A2 and COL6A2) emerge as sentinels of reductive stress.
- Reductive stress triggers receptor-independent Akt phosphorylation at Ser473.

Carne et al., 2019, Molecular & Cellular Proteomics *18*, 1123–1137

https://doi.org/10.1074/mcp.RA118.001140

Reductive Stress Selectively Disrupts Collagen Homeostasis and Modifies Growth Factor-independent Signaling Through the MAPK/Akt Pathway in Human Dermal Fibroblasts[S]

Naomi A. Carne‡, Steven Bell‡, Adrian P. Brown‡, Arto Määttä‡, Michael J. Flagler§, and Adam M. Benham‡**

Redox stress is a well-known contributor to aging and diseases in skin. Reductants such as dithiothreitol (DTT) can trigger a stress response by disrupting disulfide bonds. However, the quantitative response of the cellular proteome to reductants has not been explored, particularly in cells such as fibroblasts that produce extracellular matrix proteins. Here, we have used a robust, unbiased, label-free SWATH-MS proteomic approach to quantitate the response of skin fibroblast cells to DTT in the presence or absence of the growth factor PDGF. Of the 4487 proteins identified, only 42 proteins showed a statistically significant change of 2-fold or more with reductive stress. Our proteomics data show that reductive stress results in the loss of a small subset of reductant-sensitive proteins (including the collagens COL1A1/2 and COL3A1, and the myopathy-associated collagens COL6A1/2/3), and the down-regulation of targets downstream of the MAPK pathway. We show that a reducing environment alters signaling through the PDGF-associated MAPK/Akt pathways, inducing chronic dephosphorylation of ERK1/2 at Thr202/Tyr204 and phosphorylation of Akt at Ser473 in a growth factor-independent manner. Our data highlights collagens as sentinel molecules for redox stress downstream of MAPK/Akt, and identifies intervention points to modulate the redox environment to target skin diseases and conditions associated with erroneous matrix deposition. ***Molecular & Cellular Proteomics 18: 1123–1137, 2019. DOI: 10.1074/mcp.RA118.001140.***

Dermal fibroblasts are a heterogeneous group of cells that can be categorized into three distinct subpopulations according to their location: papillary (upper lineage), where they are more densely packed; reticular (lower lineage) where there are fewer cells among a more organized extracellular matrix (ECM)[1]; and fibroblasts associated with the hair follicle (upper lineage) (1). Skin fibroblasts play an important role in wound healing and repair and are responsible for the secretion of ECM components such as collagen and glycosaminoglycans. The secretion of collagens by fibroblasts requires a complex quality control process that begins in the endoplasmic reticulum (ER). Collagens are synthesized as procollagen α-peptides, three of which come together to form the distinctive triple-helix. The triple helix is stabilized by hydroxylation of proline and lysine residues by prolyl-4-hydroxylase (P4HA) and lysyl hydroxylase (LOX), permitting the formation of interchain hydrogen bonds. After secretion, these triple helical units assemble into ordered polymeric collagen fibrils and bundles. The fibrillar collagens (type I, II, III, V and XI) are organized into matrices in the dermis by a combination of fibrillar-associated collagens (type VI) and the contractile action of fibroblasts attached to the dispersed fibrils (2, 3).

The secretory demand to produce collagens and other ER clients can trigger an unfolded protein/ER stress response (4). A productive ER stress response results in the activation of the ER transmembrane sensors Ire1α and ATF6 to drive the production of compensatory ER chaperones and lipids, facilitating ER expansion. Meanwhile, PERK attenuates general translation while allowing the synthesis of a restricted set of target genes through the phosphorylation of eIF2α (5). ER stress responses can also feed in to cytosolic receptor mediated signaling pathways. Urano *et al.* showed that ER stress can activate the c-Jun N-terminal kinase (JNK), and that the cytoplasmic tail of IRE1 interacts with TRAF2, a JNK adaptor protein (6), most likely through ASK1, a MAPK kinase kinase (7). Thus, MAP kinases are activated by endogenous and exogenous (receptor-driven) signaling.

In addition to inducing an ER stress response, disruption of oxidative protein folding disturbs the redox balance of the cell. Reductants such as DTT can trigger an ER stress response by disrupting disulfide bonds, leading to an accumulation of newly synthesized proteins in the ER (8). However, little is

From the ‡The Department of Biosciences, Durham University, Stockton Road, Durham, DH1 3LE, UK; §The Procter & Gamble Company, 8700 Mason Montgomery Road, Mason, OH 45040

Received October 19, 2018, and in revised form, March 15, 2019
Published, MCP Papers in Press, March 19, 2019, DOI 10.1074/mcp.RA118.001140

known about the quantitative response of cells to reductants and how the global cell proteome is affected by the combined effect of redox and ER stress, particularly during metabolically demanding conditions such as proteostasis in response to growth factors. To investigate this question, we have studied the effect of reductive ER stress in human dermal skin fibroblasts subject to stimulation by PDGF. The PDGF pathway in fibroblasts is well understood and is an important contributor to wound healing in the skin. PDGF stimulates the dimerization and autophosphorylation of PDGFR family molecules, followed by recruitment of the signal transduction machinery (*e.g.* GRB2, Src, GAP, PI3 kinase, PLCγ, and NCK), culminating in the activation of STAT transcription factors. Various signaling pathways are initiated, leading to the control of cell growth, proliferation and differentiation (by src, MAPK and PKC pathways); and actin reorganization and cell migration (by the PKC and Akt/PKB pathways) (9).

Data-independent acquisition (DIA) is a robust and reproducible mass spectrometry method (10) for label-free relative quantification of all detectable analytes within a defined range based on their fragment ion spectra. Purvine *et al.* first reported a shotgun strategy to identify peptides after collision-induced dissociation in parallel on a TOF-MS machine (11). The feasibility of automating the quantitative analysis of complex peptides was demonstrated by Venable *et al.* (12) whereas an MS^E approach to simultaneously acquire exact mass values and full-scan information from complex samples at both high and low collision energy was subsequently developed by Plumb *et al.* (13). SWATH™ is a specific DIA method, which was developed by the Abersold laboratory (14) and commercialized by ABSCIEX, that we have used in this study to quantitate the response of human skin-derived (dermal) fibroblasts to reductive stress. In recent years, this methodology has been adopted to quantitate protein interactomes, to develop disease biomarkers, to reveal how organisms respond to stress and to map proteostasis, for example in fibroblasts from individuals with Down syndrome (15–18). Here, we use the technology to discover new redox-responsive protein targets that provide insight into how the redox environment could be modulated for medical and cosmetic benefit.

We find that in skin fibroblasts, reductants stimulate the chronic dephosphorylation of p42/44 MAPK (ERK1/2) while concomitantly inducing the phosphorylation of Akt in a growth factor-independent and redox-specific fashion. DIA proteomics revealed that, remarkably, only 1% of the total identified fibroblast proteome was significantly changed after chronic exposure to DTT. Of the proteins that were altered, all but one was diminished, revealing that ER stress induced by DTT does not result in the up-regulation of the pool of secretory pathway clients. Rather, reductive stress destabilizes a select set of proteins that includes collagens, ECM components and MAPK signaling pathway targets.

EXPERIMENTAL PROCEDURES

Chemicals—Standard laboratory chemicals were purchased from Sigma Aldrich, UK unless otherwise stated. LiChrosolv LC-MS chromatography solvents were from VWR, UK.

Antibodies—All primary antibodies for Western blotting were purchased from Cell Signaling, Danvers, MA unless stated otherwise. Antibodies used were: PathScan® PDGFR Activity Assay Multiplex Western Detection Mixture II (#5304, 1:2000); Phospho-p44/42 MAPK (ERK1/2) (Thr202/Tyr204) XP® rabbit mAb (#4370, 1:2000); Phospho-Akt (Ser473) (#9271, 1:1000); Akt (pan) (40D4) mouse mAb (#2920, 1:2000); Phospho-eIF2á (Ser51) rabbit pAb (#9721, 1:1000); PDI mouse mAb RL90 (ab2792, 1:100 for IF, Abcam, Cambridge, UK); β-actin mouse mAb (ab8226, 1:15000, Abcam); collagen type I goat pAb (1310-01, 1:1000 Southern Biotech, Birmingham, AL; raised by immunization against collagen type I and cross-absorped to remove any reactivity against type II, III, IV, V and VI collagens); collagen type VI rabbit pAb (14853-1-AP, 1:500, Proteintech, Rosemont, IL; raised against the human COL6A2-GST fusion protein catalogue number Ag6635). Goat anti-mouse peroxidase (GAMPO), swine anti-rabbit peroxidase (SARPO) and rabbit anti-goat peroxidase (RAGPO)-coupled secondary antibodies for Western blotting were used at 1:3000 and purchased from DAKO (Agilent, Santa Clara, CA) (#P0447, #P0217 and #P0449 respectively). Goat anti-mouse Alexa-Fluor® 488-conjugated secondary antibodies were used for immunofluorescence (Invitrogen ThermoFisher, CA). The phospho-antibodies against pPDGFR, pAkt and p44/42 were validated against a PDGF-BB stimulated fibroblast lysate (supplemental Fig. S1).

Cell Culture and Lysis—Human BJ fibroblasts were bought from ATCC®(#CRL-2522™) with initial passage number of 3, and maintained at low passage number in minimum Eagle's medium supplemented with 10% fetal calf serum, 2 mM GlutaMAX, 100 units/ml penicillin, and 100 μg/ml streptomycin (Invitrogen). Cells were passaged twice weekly, when ~90% confluent, by washing twice in sterile PBS (Sigma, St. Louis, MO or Severn Biotech, Worcestershire, UK) and dispersing in sterile trypsin (ThermoFisher) before reseeding. For cell lysis, cells were seeded in 6 cm dishes or 25 cm^2 flasks and lysates were generated by scraping cells in RIPA lysis buffer (1% v/v Triton X-100, 50 mM Tris HCl pH 8, 150 mM NaCl, 0.5% w/v Na-deoxycholate, 0.1% SDS) supplemented with 10 μg/ml of the protease inhibitors antipain, chymostatin, leupeptin and pepstatin A; and 1× phosphatase inhibitors against acid, alkaline, serine/threonine, tyrosine, and dual-specificity phosphatases (PhosSTOP, Roche, Basel, Switzerland). Lysates were cleared by centrifugation at 16,000 × *g* and post-nuclear supernatants used for subsequent analysis.

Growth Factor Stimulation—Platelet Derived Growth Factor-BB isoform (PDGF-BB, Corning #47743-598) was reconstituted in 0.1% BSA, 10 mM acetic acid. Before stimulation with PDGF-BB, spent media was removed and the cells washed with PBS. The cells were replaced into serum-free minimum Eagle's medium supplemented only with 2 mM GlutaMAX, 100 units/ml penicillin, and 100 μg/ml streptomycin (ThermoFisher), with PDGF-BB added to a final concentration of 10 ng/ml.

[1] The abbreviations used are: ECM, extracellular matrix; ATF, activating transcription factor; COL, collagen; DIA, data independent acquisition; DTT, dithiothreitol; ER, endoplasmic reticulum; ERK, extracellular signal-regulated kinase; FCS fetal calf serum; GAMPO, goat anti-mouse peroxidase; MAPK, mitogen activated protein kinase; PDGFR, platelet derived growth factor; PDI, protein disulfide isomerase; PERK, PKR-like endoplasmic reticulum kinase; RAGPO, rabbit anti-goat peroxidase; RIPA, radio-immunoprecipitation assay; SARPO, swine anti-rabbit peroxidase; SFM, serum free media; STAT, signal transducer and activator of transcription; SWATH, sequential windowed acquisition of all theoretical fragment ion mass spectra.

Protein Analysis—Protein concentration was calculated using an acidified Bradford assay or the commercially available Pierce™ BCA assay kit (ThermoFisher Scientific, 23225). For the Bradford assay, a standard curve was prepared using 10 μl 0, 1, 2, 5, 8, and 10 μg/ml bovine serum albumin (BSA) in RIPA buffer, and samples were prepared as 2 μl sample, 8 μl RIPA buffer. These were each added to 10 μl 0.1 M HCl, 80 μl water and 900 μl Bradford dye (BioRad, Hercules, CA), vortexed and incubated at room temperature for 10 min. Absorbance was read at 595 nm using an Eppendorf Biophotometer for the Bradford assay (Eppendorf AG, Hamburg, Germany). The BCA assay was performed according to manufacturer's instructions in a microplate.

SDS-PAGE and Western Blotting—Postnuclear supernatants were taken up in 2× sample buffer (65.8 mM Tris, pH 6.8, 2.1% SDS, 26.3% glycerol, 50 mM DTT and 0.01% bromphenol blue), denatured at 95 °C for 5 min, and then subjected to 10% SDS-PAGE. Gels were transferred to polyvinylidene fluoride (PVDF) membranes (Millipore) for 2 h at 150 mA or 30 V overnight, and then blocked in 5% milk in TBS-Tween for 1 h at room temperature or 8 h at 4 °C. Membranes were incubated with primary antibodies in 5% BSA or 5% milk in TBS-Tween overnight at 4 °C before being washed five times with TBS-Tween. Membranes were then incubated with GAMPO, RAGPO or SARPO secondary antibodies for 1 h at room temperature and washed a further five times with TBS-Tween. Proteins were visualized with 500 μl enhanced chemiluminescence fluid (GE Healthcare, IL) per membrane and exposed to film (Kodak) before development in an X-ray developer machine (XOMAT).

Senescence Associated β Galactosidase Activity assay—Staining for senescence-associated β-galactosidase activity was performed using the Senescence β-Galactosidase Staining Kit from Cell Signaling (9860) according to the manufacturer's instructions. Briefly, spent media from treated BJ fibroblast cells was removed and cells were washed once with PBS before fixing in a proprietary fixative solution for 10–15 min at room temperature. Cells were then washed a further two times before application of pH-adjusted β-galactosidase staining solution and incubated overnight in a dry incubator at 37 °C. Staining solution was then removed, and cells washed twice with PBS. Following staining, dishes of stained cells were either stored in glycerol at 4 °C or immediately DAPI stained and cover slips mounted on microscope slides for analysis. Images were taken using a CMEX WiFi 5 camera (Euromex, DC.5000-WIFI) attached to an inverted wide field fluorescence microscope for analysis of DAPI stained cells (Zeiss Apotome).

Wound Closure Assay—The wound closure assay was performed according to the method of Liang *et al.* (19). BJ fibroblasts were seeded onto 6-well plates (Greiner) which had been pre-treated with 10 μg/ml fibronectin (Sigma) and grown to confluency. Cells were serum starved for 24 h and the bottom of each well was scratched with a pipette tip (0.2 ml) to create a linear wound area free of cells. After washing twice with PBS (ThermoFisher) the cells were incubated in 10 ng/ml PDGF supplemented culture media ± 5 mM DTT (Sigma). After 10 min, the cells were washed and fresh SFM containing 10 ng/ml PDGF was added. Cell migration was recorded with an automated Zeiss Cell Observer for 12 h with images taken every 30 min. The cells were kept at 37 °C and 5% CO_2 during image capture. Cell viability was confirmed by monitoring cell movement. Migration into the wound site was quantified by counting how many cells passed the scratch point after 10 h; and by calculating the percentage of cells in the field of view that had passed the scratch point after 10 h. A 1-way ANOVA with a Dunnett's multiple comparison test was conducted in Prism 8 to assess statistical significance (mean ± S.D., $n = 3$).

Immunofluorescence—Cells for analysis by immunofluorescence were seeded onto coverslips in 6 cm dishes before treatment. Treatments were performed once cells had reached ~80% confluence, after which the cells were washed twice with PBS containing 1 mM $CaCl_2$ and 0.5 mM $MgCl_2$ (PBS^{++}). Cells were fixed for 10 min in 4% paraformaldehyde, washed in PBS^{++}, permeabilized using 0.1% Triton X-100 for 10 min, washed once for 5 min with PBS^{++} and blocked with 2% BSA for 1 h at room temperature. Coverslips were incubated with the anti-PDI antibody RL90 at 1:100 dilution in PBS^{++}/0.2% BSA overnight at 4 °C. The cells were washed in PBS^{++} and then incubated with Alexa-Fluor® 488-conjugated secondary antibody (Invitrogen ThermoFisher) for 1 h at room temperature. The cells were washed three times in PBS^{++} and stained with DAPI to visualize nuclei (Sigma). The immunofluorescence images were captured with a brightfield fluorescence microscope (Zeiss Axio Imager M1).

RT-PCR and XBP1 Assay—Cells (~10^6 in a 25 cm^2 flask) at ~90% confluence were subjected to a 1 h or 6 h stress with 5 mM DTT in the presence or absence of 10 ng/ml PDGF stimulation for 24 h. Cells were washed twice in PBS, lysed in 300 μl TRI reagent and RNA extracted with 50 μl chloroform. RNA content was measured using an ND-1000 spectrophotometer (Nanodrop® Technologies Inc) and 50 ng RNA was subjected to RT-PCR, using the Access-Quick RT-PCR kit (Promega). Primers for Actin were: CCACACCTTCTACAATGAGC and ACTCCTGCTTGCTGATCCAC and for XBP1 were: GAAACTGAAAAACAGAGTAGCAGC and GCTTCCAGCTTGGCTGATG. PCR was carried out using a PTC-200 DNA engine (MJ Research) with 30 cycles of 94 °C for 30 s, 60 °C for 1 min, and 72 °C for 1 min. Actin cDNA was analyzed on a 1% agarose gel whereas XBP1 cDNA was subjected to Pst1 digestion for 2 h at 37 °C and DNA purified using a PCR purification kit (Qiagen, Hilden, Germany) to distinguish between the IRE1-spliced and non-spliced forms of XBP1. The resulting digested cDNA was then analyzed on a 2% agarose gel and both 1 and 2% gels were visualized by UV light with an INGenius bioimager (Syngene). White on black images were inverted using ImageJ software.

Proteomics and Mass Spectrometry—Peptide samples were prepared using a commercial FASP Protein Digestion Kit (Expedeon #44250) and sequencing grade-modified trypsin (Promega, #V5111). Spin-filter eluates were freeze-dried and resuspended in 3% acetonitrile, 0.1% TFA and de-salted using C18 ZipTips (Millipore). Sample fractions containing 5 μg peptides were analyzed using an ekspert™ nanoLC 425 with low micro gradient flow module (Eksigent) coupled to a quadrupole Time-Of-Flight (QTOF) mass spectrometer (TripleTOF 6600, SCIEX, MA) with a DuoSpray source (SCIEX) and a 50-micron ESI electrode (Eksigent). Samples were loaded and washed on a TriArt C18 Capillary guard column 1/32″, 5 μm, 5 × 0.5 mm trap column (YMC) and online chromatographic separation performed over 57 min on a Triart C18 Capillary column 1/32″, 12 nm, S-3 μm, 150 × 0.3 mm (YMC) at a flow rate of 5 μl/min with a linear gradient of 3–32% acetonitrile, 0.1% formic acid over 43 min, then to 80% acetonitrile, 0.1% formic acid over 2 min, held for 3 min before returning to 3% acetonitrile, 0.1% formic acid and re-equilibrated. SWATH acquisition was for 55 min with a 3.2 s cycle time. Each cycle consisted of MS-spectrum acquisition at 400 to 1,250 *m/z* for 250 msec followed by MS/MS (100 to 1500 *m/z*) using 100 variable SWATH windows (parameters downloaded from http://sciex.com/community/entitty/1217), 25 msec accumulation for each in high sensitivity mode with rolling CE and 2+ ions selected. Analyst software version 1.7.1 (SCIEX) was used to acquire all MS and MS/MS data. Samples were spiked with iRT peptides (Biognosys) at a ratio of 1 μg protein to 0.1 μl 10 × RT peptide mix.

Experimental Design and Statistical Rationale—Three biological and three technical replicates were obtained for each treatment condition, widely accepted as appropriate to permit the use of statistical tests in analysis. Protein identifications were obtained by searching spectra against the 10316 entries in the panhuman 10000 protein 2014 spectral library PDX000954 (20) in PeakView version 2.2 with the

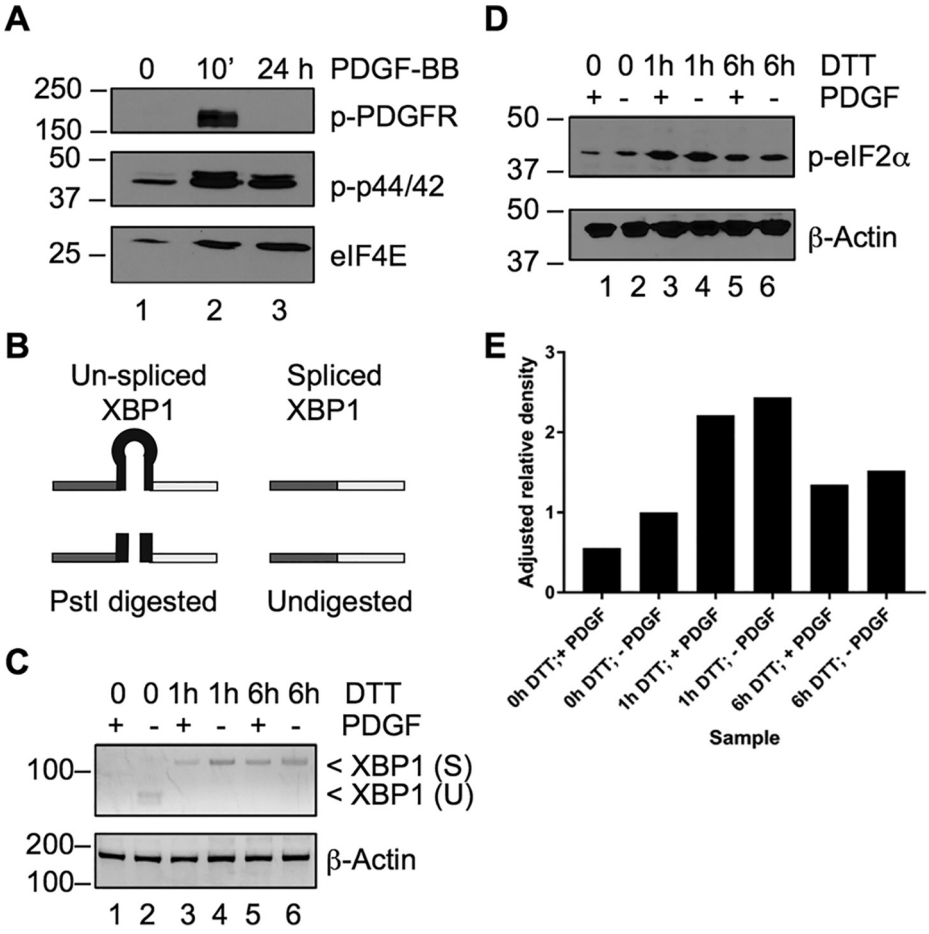

FIG. 1. **PDGF signaling and induction of an ER stress response in BJ Fibroblasts.** *A*, Lysates from BJ fibroblasts treated with 10 ng ml^{-1} PDGF-BB for 10′ or 24 h in serum free media were analyzed by 10% SDS-PAGE followed by immunoblotting for p-PDGFR, p-p44/42 and eIF4E. PDGF-BB initiated a signaling response within 10′. A representative image of $n = 3$ biological replicates is shown; kDa markers are shown on the left. *B*, Schematic RT-PCR assay illustrating the expected PCR products of XBP1 depending on splicing/activation status. When XBP1 is activated by ER stress, the PstI restriction site is removed and PstI digestion no longer occurs. *C*, RT-PCR products from BJ fibroblasts treated ± 10 ng ml^{-1} PDGF-BB ± DTT were analyzed by 2% agarose gel electrophoresis following digestion with PstI for the expression of XBP1 (upper panel) and β Actin (lower panel). DTT resulted in the splicing of XBP1. bp markers are shown on the left. *D*, Lysates from BJ fibroblasts treated ± 10 ng ml^{-1} PDGF-BB for 24 h in serum free media ± DTT were analyzed by 10% SDS-PAGE followed by immunoblotting for p-eIF2α (upper panel) and actin (lower panel). DTT, but not PDGF-BB alone, stimulated the phosphorylation of eIF2α. kDa markers are shown on the left. *E*, Relative quantitation of the p-eIF2α levels shown in (*D*)

MS/MS^{ALL} with SWATH™ acquisition microapp version 2.0. Chromatographic retention time calibration was performed using iRT peptides, and SWATH data processing carried out with the default settings as advised by SCIEX (300 peptides per protein, 5 transitions per peptide, 95% peptide confidence threshold, 1% peptide false discovery rate threshold, 3.0 XIC extraction window and XIC width 75 ppm). Following processing, data was exported to MarkerView version 1.2.1 and normalized by total area sums before analysis by *t* test. FDR correction of *t* test associated *p* values was performed using the p.adjust function in R. Co-efficient of variance calculations were performed using peak area values for each protein manually in excel. R was used to produce graphics. Statistical testing for overrepresentation or enrichment of GO terms was performed using the Panther tools available at pantherdb.org including Bonferroni correction for multiple testing (21). The mass spectrometry data have been deposited to the ProteomeXchange Consortium via the PRIDE (20) partner repository with the data set identifier PXD010747.

RESULTS

DTT Induces ER Stress in Fibroblasts in the Presence or Absence of PDGF—PDGF proteins occur as a family of disulfide-bonded, dimeric isoforms (PDGF-AA, AB, BB, CC and DD). For our experiments, we stimulated cells with PDGF-BB, because this isoform binds to PDGFRαβ, αα and αβ receptor combinations (22). Further, PDGF-BB is known from the literature to stimulate the fibroblasts used in this study, and exogenous PDGF-BB is effective in promoting wound healing *in vitro* and in ameliorating wound healing disorders *in vivo* (23, 24). Initial experiments confirmed that the application of PDGF-BB to serum-starved cultured skin fibroblasts resulted in the transient phosphorylation (within 10 min) of PDGFRβ at Tyr751, at the docking site for PI3 kinase (Fig. 1*A*, upper panel). PDGF-BB also resulted in a rapid increase in the phosphorylation of ERK1/2 (p44/p42) at Thr202/Tyr204 (Fig. 1*A*, middle panel), indicating that a signaling response was initiated upon growth factor exposure. An antibody against eIF4E was used as a loading/blotting control (Fig. 1*A*, lower panel).

PDGF stimulates cell growth and proliferation and therefore may place demands on the oxidative protein folding machinery in the ER. To assess whether long-term (24 h) PDGF stimulation caused an ER stress response or altered the effects of DTT treatment, fibroblasts were serum-starved ± PDGF stimulation ± DTT for 1 h or 6 h and assayed for the activation of the ER stress marker XBP1 (25). We took advantage of a unique Pst1 restriction site within the intron of XBP1 to differentiate between un-spliced (inactive) and spliced (active) forms of XBP1 by RT-PCR (Fig. 1*B*). RT-PCR products were digested for 2 h with Pst1 before analysis on 2% agarose gel. Cells were exposed to a total of 24 h PDGF-BB, with DTT (when present) being added 1 or 6 h before the end of this

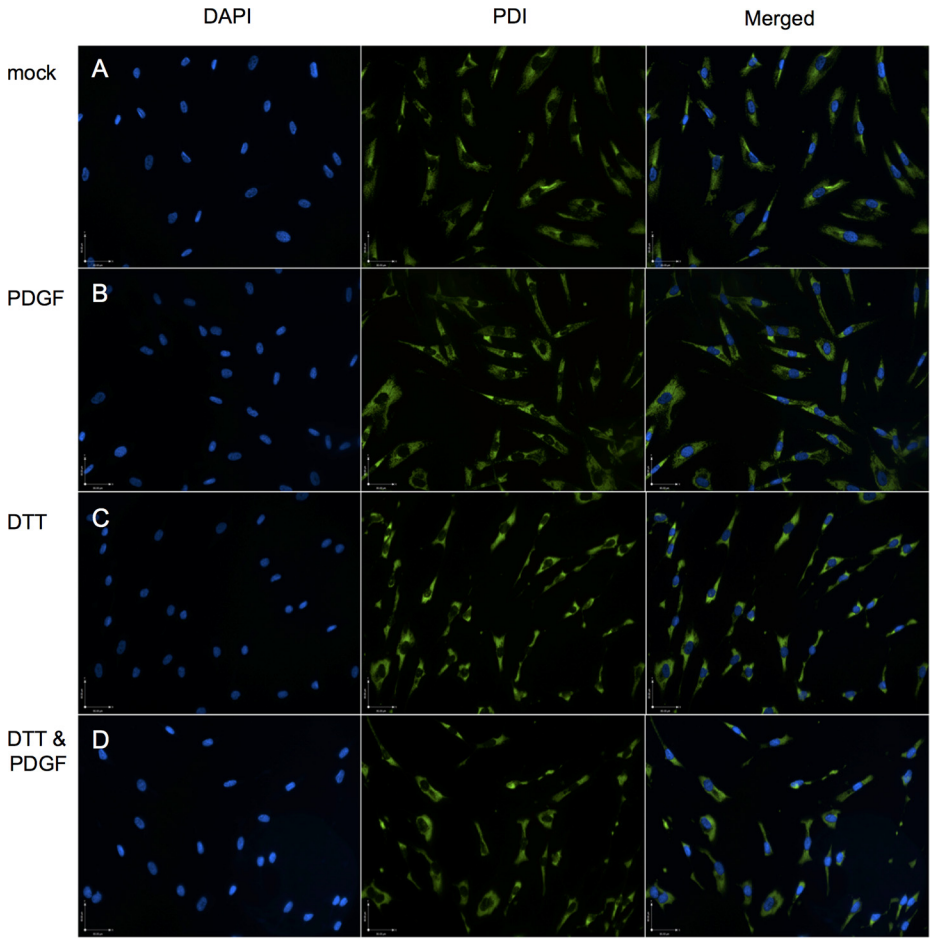

FIG. 2. **Treatment of BJ fibroblasts with PDGF and/or DTT does not alter the gross morphology of fibroblasts.** Cells were incubated in serum free media for 24 h with (*A*) no additional treatment, (*B*) 6 h 5 ng ml^{-1} PDGF-BB beginning at $t = 18$ h, (*C*) 6 h 5 mM DTT beginning at $t = 18$ h, or (*D*) 6 h 5 ng ml^{-1} PDGF-BB and 5 mM DTT beginning at $t = 18$ h before fixing and staining for DAPI and PDI. Stained cells were then imaged at 20× magnification with a brightfield fluorescent microscope. Scale bar represents 10 microns.

time to allow an initial response to PDGF stimulation that was uninhibited by the addition of DTT. In fibroblasts subjected to DTT for 1 h or 6 h, a single ~100 bp band was seen, indicative of an ER stress response (Fig. 1*C*, lanes 3–6). In the absence of DTT, ER stress was not induced (Fig. 1*C*, lanes 1–2). DTT activated XBP1 splicing regardless of whether PDGF was present (compare Fig. 1*C*, lanes 5 and 6) and PDGF treatment alone did not induce XBP1 splicing (Fig. 1*C*, lane 1). Actin was used as an expression control (Fig. 1*C*, lower panel). Under conditions of ER stress, eIF2α is phosphorylated by PERK to inhibit general protein translation (26). Thus to determine whether the PERK branch of the UPR was activated by PDGF or DTT, the phosphorylation of the initiation factor eIF2α was assessed, with actin used as a Western blotting control. Whereas PDGF alone did not increase the basal phosphorylation of eIF2α at Ser51 (Fig. 1*D*, compare lanes 1 and 2), DTT did increase the phosphorylation of eIF2α after both 1 h and 6 h of treatment (Fig. 1*D*, lanes 3–6 and Fig. 1*E*). Further, cells subjected to DTT, PDGF, and DTT and PDGF combined remained viable and adherent, as judged by immunofluorescence analysis of cells with the ER resident protein PDI and the nuclear marker DAPI (Fig. 2).

DIA Quantitative Proteomic Analysis of Reductively Stressed Fibroblasts—Having demonstrated that DTT treatment induces an unfolded protein response in viable cells that is independent of PDGFR growth factor signaling, we sought to analyze and relatively quantitate the response of the fibroblast proteome to reductive stress, in a label free and unbiased manner. BJ fibroblasts were cultured for 24 h in serum free media either alone (untreated), with 5 mM DTT for 6 h (DTT only), with 10 ng/ml PDGF-BB in serum free media (PDGF only) or with PDGF-BB in the serum free media and 5 mM DTT for 6 h. Following treatments, three biological replicates of each condition were lysed in RIPA buffer and prepared for quantitative DIA mass spectrometry analysis using filter-aided sample preparation (FASP). Three technical replicate LC-MS runs were undertaken for each biological replicate providing 9 replicates for each condition (Fig. 3*A*). A total of 4487 proteins were quantified using this method. Of the significantly changed proteins, 12 arose from single peptide identifications. Seven of these 12 proteins (MXRA8, IGF2, WNT5A, CD248, LOX, UBL5, and CMTM6) had clear, reproducible peaks on analysis of the ion chromatograms (supplementary data). Five identifications had weak peaks on analysis of the extracted ion chromatograms. These 5 proteins (FKBP11, TOR4A, OCIAD2, CDKN1A, and GAS6) were therefore excluded from further analysis. Overall, forty-one proteins showed a significantly decreased (FDR adjusted $p < 0.05$) fold change (FC) greater than 2 with DTT treatment alone (Fig. 3*B*),

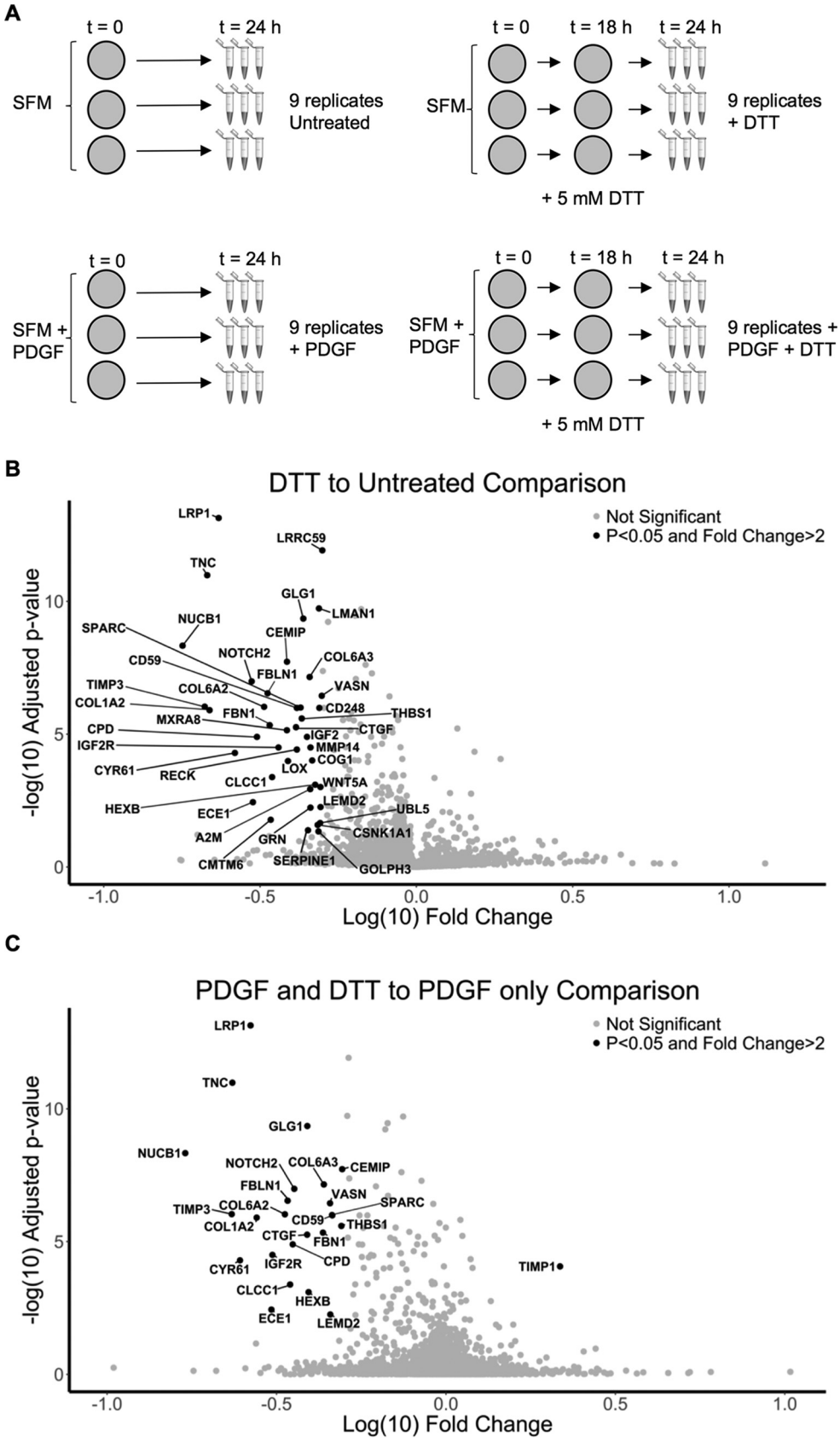
A
t = 0
t = 24 h
SFM
9 replicates
Untreated
t = 0
t = 18 h
t = 24 h
SFM
9 replicates
+ DTT
+ 5 mM DTT
t = 0
t = 24 h
SFM +
PDGF
9 replicates
+ PDGF
t = 0
t = 18 h
t = 24 h
SFM +
PDGF
9 replicates +
PDGF + DTT
+ 5 mM DTT
B
DTT to Untreated Comparison
Not Significant
P<0.05 and Fold Change>2
-log(10) Adjusted p-value
Log(10) Fold Change
LRP1
LRRC59
TNC
GLG1
LMAN1
NUCB1
SPARC
CEMIP
NOTCH2
COL6A3
CD59
FBLN1
TIMP3
COL6A2
VASN
COL1A2
FBN1
CD248
THBS1
MXRA8
CTGF
CPD
IGF2
IGF2R
MMP14
COG1
CYR61
RECK
LOX
CLCC1
WNT5A
HEXB
LEMD2
UBL5
ECE1
CSNK1A1
A2M
GRN
CMTM6
SERPINE1
GOLPH3
C
PDGF and DTT to PDGF only Comparison
Not Significant
P<0.05 and Fold Change>2
-log(10) Adjusted p-value
Log(10) Fold Change
LRP1
TNC
GLG1
NUCB1
NOTCH2
COL6A3
CEMIP
FBLN1
VASN
TIMP3
COL6A2
SPARC
CD59
COL1A2
THBS1
CTGF
FBN1
CYR61
IGF2R
CPD
TIMP1
CLCC1
HEXB
ECE1
LEMD2

and 24 proteins showed a significant FC>2 decrease with DTT and PDGF together (Fig. 3*C*; see also supplementary excel file). Only one protein, TIMP1, significantly increased in abundance > 2-fold upon reductive stress in the presence of PDGF. To determine the robustness of the quantitative data obtained, the coefficient of variance was determined for the quantified values for each protein across all 9 replicates. This provides a measure of the variance in the quantified values as a percentage of the mean. An average of 76.8% identifications were found to have %CV ≤ 20% and 89.4% identifications had %CV ≤ 30% to account for the increased variability expected in biological replicates (supplemental Fig. S2).

The 41 proteins identified as decreasing in the two groups overlapped almost completely; however, in most cases, treatment with PDGF in addition to DTT slightly reduced the fold change, indicating that PDGF had a mild dampening effect on the outcome of DTT exposure. There was an additional set of 17 proteins that significantly declined >2-fold only in the presence of DTT alone, including the plasma membrane recycling receptor CMTM6, the matrix metalloprotease regulator RECK, the serine protease inhibitor and regulator of cell migration SERPINE1, and regulators of the insulin growth factor pathway (IGF2 and MXRA8). The fold changes in global expression of statistically significant proteins that decreased with DTT alone (*versus* DTT and PDGF treatment) are compared in a heat map (Fig. 4*A*).

The GO terms annotated to the proteins identified as significantly changing in response to DTT treatment were next tested for statistical overrepresentation using the Panther overrepresentation test (Fig. 4*B*). Regulation of ERK1/2 and MAPK were overrepresented in the significantly changing proteins from DTT treatment, both with and without PDGF. This reveals that proteins involved in ERK1/2 regulation are disproportionately downregulated compared with the total quantifiable proteome detected in this study. ERK1/2 (p44/42) are MAP kinases that are activated by growth factors, and promote cell proliferation, cell survival and migration. In DTT treated cells, with and without PDGF, the proteins annotated to this term were CYR61, NOTCH2, CTGF, TIMP3, and FBLN1. CYR61 has been linked to induction of the ERK1/2 cascade in osteosarcoma cells undergoing epithelial to mesenchymal transition (EMT) (27); inactivation of ERK1/2 inhibited the Jagged/Notch signaling pathway in lens epithelial cells (28); and ERK1/2 signaling was shown to upregulate CTGF in the mediation of myocardial fibrosis (29). Because an increase in ERK1/2 signaling is associated with the increase in expression of these proteins in the cited literature, we reasoned that down-regulation of these proteins would be associated with a decrease or perturbation in ERK1/2 (MAPK) signaling. The ERK1/2 scaffold proteins paxillin (PXN), flotillin-1 (FLOT1), MEK binding partner 1 (MP1) and Ras GTPase-activating-like protein IQGAP1 were identified in the data, however the relative levels of these proteins did not change significantly with treatment (supplementary data). This suggests that any differences in ERK1/2 signaling are unlikely to have been mediated by scaffold protein abundance.

Reducing Conditions Induce the Long-term Dephosphorylation of MAPK p42/44—To confirm the quantitative DIA analysis and to test the hypothesis that reductants lead to alterations in MAPK signaling pathways, we combined PDGF stimulation with DTT treatment for 1 h or 6 h as before (Fig. 5*A*) and analyzed the protein lysates for the induction of phosphorylated p44/42 (ERK1/2) and phosphorylated Akt by Western blotting (Fig. 5*B*). Akt is a PDGF stimulated signaling molecule that regulates cell proliferation and survival downstream of ERK1/2. Fig. 5*B* shows that a chronic 6 h reductive stress was enough to downregulate phosphorylation of ERK1/2 at Thr202/Tyr204, both with or without PDGF stimulation (Fig. 5*B*, first panel, lanes 5 and 6). Concurrently, Akt phosphorylation at Ser473 was promoted, even in the absence of PDGF (Fig. 5*B*, second panel, lanes 5 and 6). In contrast, as anticipated from the DIA proteomic results, the overall protein expression levels of the ER chaperones BiP (HSPA5) and gp96 (HSP90B1) were not elevated by treatment with PDGF or DTT (Fig. 5*B*, third and fourth panel), like the eIF4E control (Fig. 5*B*, fifth panel). The Akt signaling response also occurred when serum was present in the growth media but was not induced by the senescence promoting reagent etoposide (Fig. 5*C*, compare lanes 1–3 with 4–6). These experiments corroborate the independent DIA data (Figs. 3 and 4) and show that reductants dynamically regulate growth factor independent MAPK/ERK signal transduction through the phosphorylation of intermediary molecules.

DTT Induces Chronic Akt Phosphorylation That Can Be Prevented by the Akt Inhibitor Perifosine—To further understand the flux through MAPK/Akt that occurs in response to DTT, a time-course was performed, gathering lysates from time-points between 10 min and 6 h after DTT application, in the absence of PDGF stimulation. ERK1/2 phosphorylation was initially stimulated above background by DTT at 10 min, but was gradually attenuated, with a noticeable decline first seen by 4 h (Fig. 6*A*, upper panel, lanes 6–7). No phosphorylation of Akt was seen at 0 min DTT treatment (Fig. 6*A*, middle panel, lane 1) consistent with Fig. 5*B*. Phosphorylation of Akt was first seen after 1 h in the presence of DTT and the signal continued to gain in intensity until 6 h (Fig. 6*A*, middle

FIG. 3. **Proteomic analysis of fibroblasts subjected to DTT treatment ± PDGF.** *A*, Schematic showing BJ fibroblasts serum-starved for 24 h ± 10 ng ml^{-1} PDGF-BB and treated for 6 h ± 5 mM DTT. Lysates from 3 biological replicates and 3 technical replicates were used for SWATH acquisition. *B* and *C*, Identification of proteins and relative quantitation was achieved by MS analysis using SWATH acquisition on a TripleTOF 6600 (SCIEX). Log10(*p* value) was plotted against Log10(Fold change). Proteins displaying a significant (FDR-adjusted $p < 0.05$) fold change > 2 are labeled on the volcano plots.

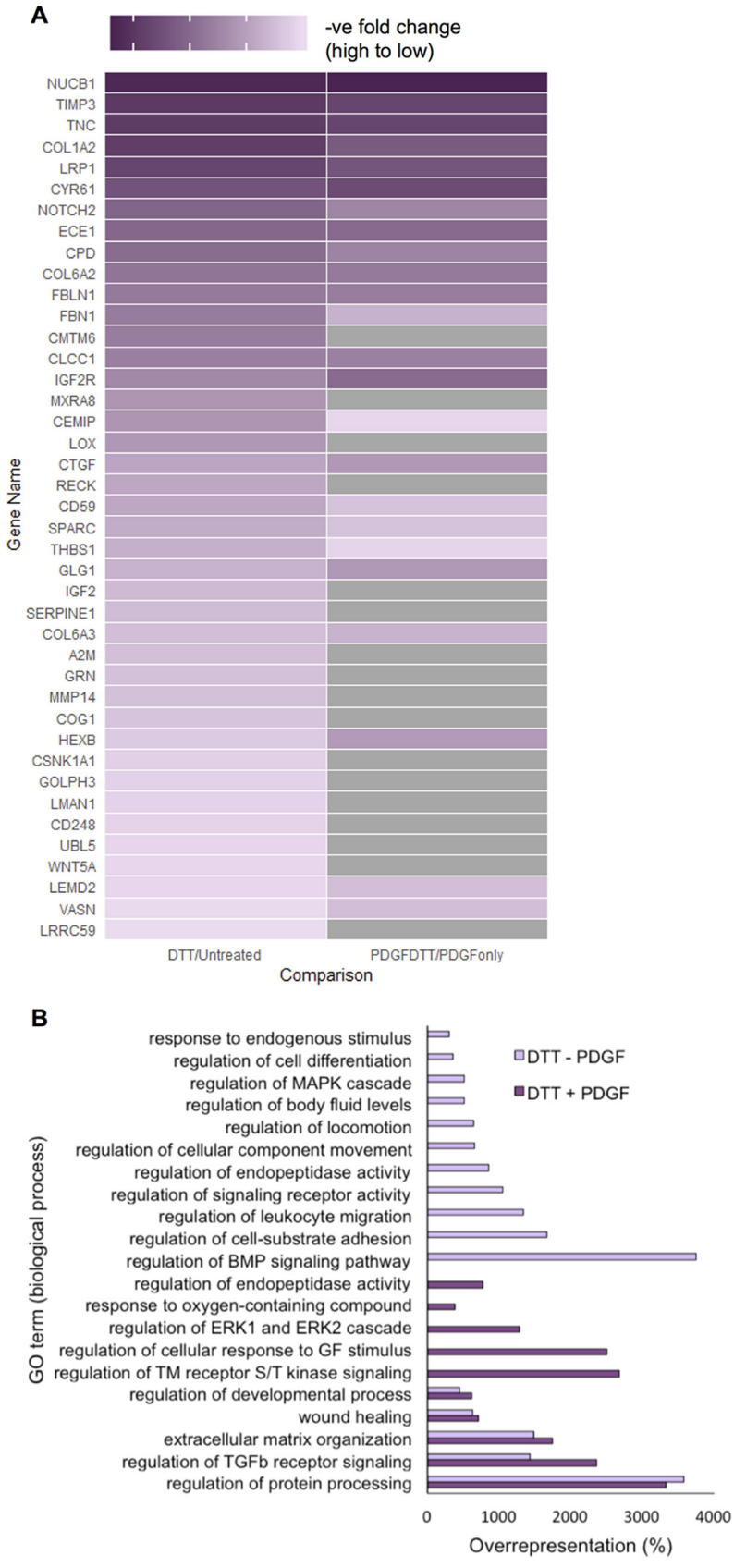

FIG. 4. **Identification of downregulated MAPK targets and ECM proteins.** *A*, The heat map shows the fold change of significantly downregulated proteins, compared between +DTT and +DTT +PDGF. *B*, Percentage overrepresentation of GO biological process terms found to be statistically significantly overrepresented upon DTT treatment. Proteins were tested against a reference list of all quantified proteins in the data set using the PANTHER overrepresentation test (release 20171205) and PANTHER version 13.1 (release 2018-08-09). A Fisher's exact test with FDR multiple test correction was carried out using the GO biological process complete annotation set. For ease of viewing only the parent GO term is displayed and organ-specific terms have been removed.

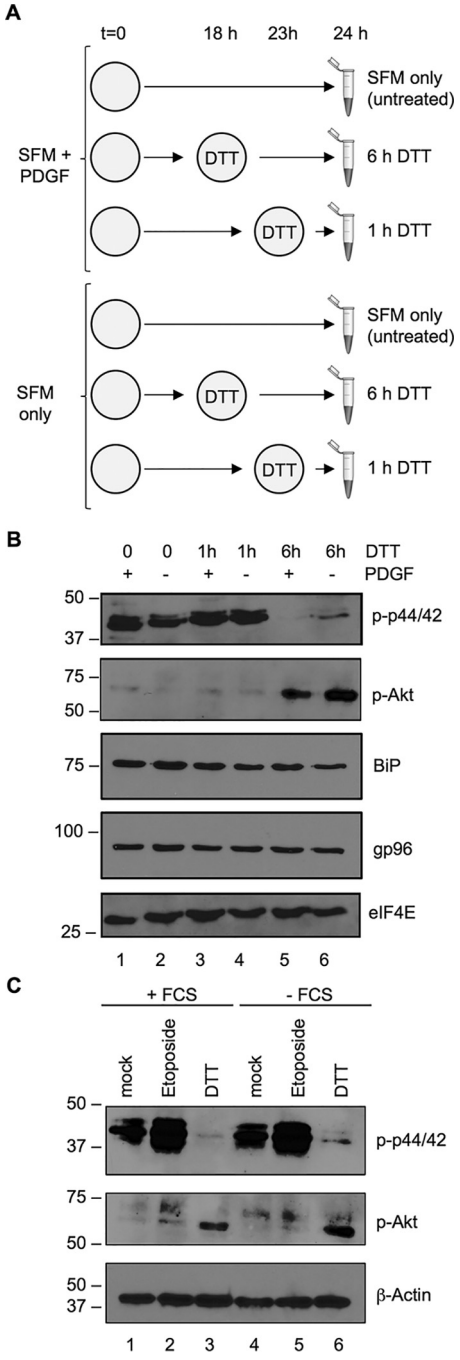

FIG. 5. **DTT stimulates Akt phosphorylation in the absence of PDGF.** *A*, BJ fibroblasts were treated for 0, 1, or 6 h with 5 mM DTT in serum free media ±10 ng ml^{-1} PDGF-BB. *B*, Lysates were analyzed by 10% SDS-PAGE and immunoblotted with antibodies against p-p44/42, p-Akt, BiP, gp96 and eIF4E. *C*, Lysates from BJ fibroblasts treated for 6 h with 12.5 μM etoposide or 5 mM DTT in serum-containing (+FCS) or serum free conditions (-FCS) were analyzed by 10% SDS-PAGE and immunoblotted for p-p44/42, p-Akt and β-Actin.

panel, lanes 4–9) whereas levels of total Akt remained constant (Fig. 6*A*, lower panel). Thus, DTT induced sustained, long-term dephosphorylation of MAPK and phosphorylation of Akt.

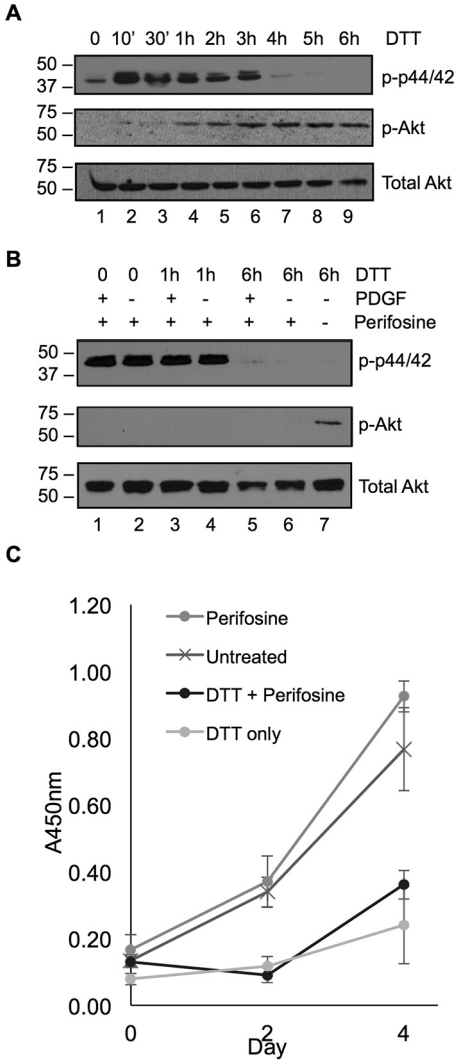

FIG. 6. **Akt phosphorylation is chronically induced by DTT.** *A*, Lysates from BJ fibroblasts treated with 5 mM DTT (in the absence of PDGF) were analyzed by 10% SDS-PAGE followed by immunoblotting for p-p44/42, p-Akt or total Akt. *B*, Lysates from BJ fibroblasts treated with perifosine in addition to DTT ± PDGF were analyzed by 10% SDS-PAGE and immunoblotted for p-p44/42, p-Akt, and total Akt. *C*, Representative images from $n = 2$ biological replicates. Proliferation of cells treated with DTT in the presence or absence of perifosine was assayed with the Orangu™ proliferation assay, measuring absorbance at 450 nm. Error bars represent 1 S.D. away from the mean.

To further explore the induction of Akt phosphorylation by reductive conditions, cells were treated with the alkylphospholipid Akt inhibitor perifosine in the presence or absence of PDGF before DTT exposure. The phosphorylation of p44/42 disappeared after 6 h, as seen previously (Fig. 6*B*, upper panel). However, perifosine inhibited the phosphorylation of Akt and ablated the signal seen in the presence of DTT alone, whereas total Akt levels remained constant (Fig. 6*B*, middle and lower panels). Perifosine treatment did not affect cell proliferation, either with or without DTT, as measured by a cell

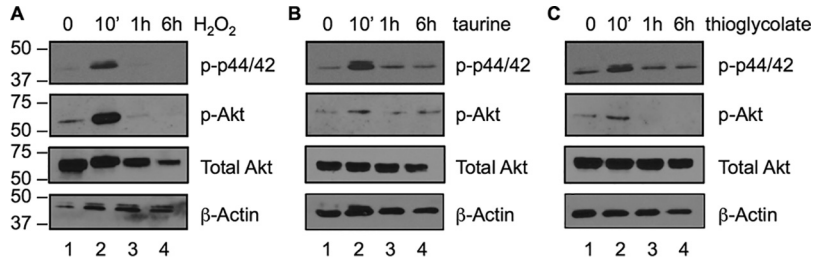

FIG. 7. **Signaling responses to redox reagents.** Lysates from BJ fibroblasts treated with 5 mM hydrogen peroxide (*A*), 5 mM taurine (*B*) or 5 mM thioglycolate (*C*) were analyzed by 10% SDS-PAGE followed by immunoblotting for p-p44/42, p-Akt, total Akt or β-Actin. Representative images from $n = 2$ biological replicates.

proliferation assay (Fig. 6*C*) and did not enhance cell death or senescence, as judged by a senescence associated βGal assay (supplemental Fig. S3). This suggests that, unlike perifosine anti-cancer combination therapies (30), DTT does not synergize with perifosine to promote cell death of skin fibroblasts. Taken together, the data imply that mild reductive stress may, in fact, stimulate a pro-survival MAPK/Akt signaling response.

To test the hypothesis that transient stimulation with reductants can simulate cell migration, we performed a cellular scratch-wound assay (supplemental Fig. S4). PDGF stimulated fibroblasts were assessed for their ability to migrate into a wound site with or without a pulse of DTT. After a DTT pulse, 62% cells migrated after 10 h post-wounding, whereas only 45% of cells migrated in the absence of DTT. This result demonstrates that an acute reductive stimulus can promote biological outcomes downstream of ERK signaling pathways.

A Range of Reductants and Antioxidants Modulate Receptor-independent p-44/42 and Akt Phosphorylation—To establish whether signal transduction through the MAPK/Akt pathway was specifically influenced by DTT, or was generally sensitive to redox perturbations, the effects of taurine and thioglycolate were investigated. The β-amino acid taurine, also known as 2-aminoethanesulfonic acid, is a potent antioxidant that occurs naturally during methionine and cysteine metabolism. It is involved in detoxification (31, 32) and has anti-fibrotic properties that have led to its use in cosmetics and anti-aging creams. Thioglycolate is present in many depilatory products used for cosmetic hair removal and reduces disulfide bonds in keratins to weaken hair structure (33). Peroxide was used as a control to induce oxidative stress, as H_2O_2 has previously been shown to induce Akt phosphorylation (34).

BJ fibroblasts were treated with 5 mM taurine, 5 mM thioglycolate, or 5 mM H_2O_2 for 10 min, 1 h or 6 h. Cells were then lysed in RIPA buffer and the lysates analyzed by immunoblot for p-p44/42 and p-Akt. As expected, H_2O_2 induced a rapid increase in both p44/42 and Akt phosphorylation within 10 mins and this declined following long-term exposure (Fig. 7*A*). Both taurine (Fig. 7*B*) and thioglycolate (Fig. 7*C*) also induced an increase in phosphorylated p44/42 and Akt by 10 mins followed by a decline within 1 h. Total Akt (Fig. 7*A*–7*C*, third panel) and β-actin (Fig. 7*A*–7*C*, fourth panel) were used as blotting and loading controls in these experiments. DTT, taurine and thioglycolate all induced p44/42 and Akt phosphorylation, but the response to taurine and thioglycolate was more rapid and transient than the response to DTT, where there was a lag in Akt phosphorylation (compare Fig. 6*A* with Fig. 7*B* and 7*C*). Taken together, these findings demonstrate that growth factor independent signaling through the MAPK pathway is induced by a range of reducing and oxidizing agents, with some temporal differences in dynamics that may be dependent on effective concentration or reduction potential.

Collagen Homeostasis is Selectively Perturbed by DTT—Having uncovered novel signaling events in skin fibroblasts in response to reductants from the DIA proteomic analysis, we further explored the long-term consequences of reductive stress for the global proteome. Several GO terms overrepresented in the DTT responding protein data set (Fig. 4*B*) were associated with modification of the ECM. These included 'extracellular matrix organization' and "wound healing" (overrepresented both with and without PDGF). This data suggested that reductants disproportionately influence the quantity and quality of ECM proteins secreted by fibroblasts and do not indiscriminately disrupt the levels of all secretory pathway/plasma membrane localized proteins.

To analyze this further, the protein identifications and their respective fold change values for each data set (DTT *versus* Untreated and PDGF/DTT *versus* PDGF only) were investigated for statistically significant enrichment of GO terms. Using the PANTHER GO Slim annotation for biological process, a significant enrichment was seen for the term 'biological adhesion' only in the DTT to Untreated comparison (Fig. 8*A*). Fig. 8*A* shows the cumulative fraction of all proteins identified in the DTT to untreated comparison (*y* axis) plotted against the corresponding uploaded value of fold change (*x* axis) in blue. The values for those proteins annotated to the term 'biological adhesion' are similarly plotted in red. The shift of this curve to the left indicates lower values of fold change associated with proteins mapped to this term. There were 119 such proteins in this data set including, for example, ECM collagens, cell junction proteins (including integrins and cadherins), and signaling proteins, such as the Ras related protein RAP1A. The enrichment shows that the distribution of proteins annotated to this term is shifted more toward the lower values than the overall distribution pattern of all proteins. This suggests that proteins associated with "biological adhesion" are disproportionately downregulated following DTT treatment compared with the global proteome response. Among the 18 collagen proteins

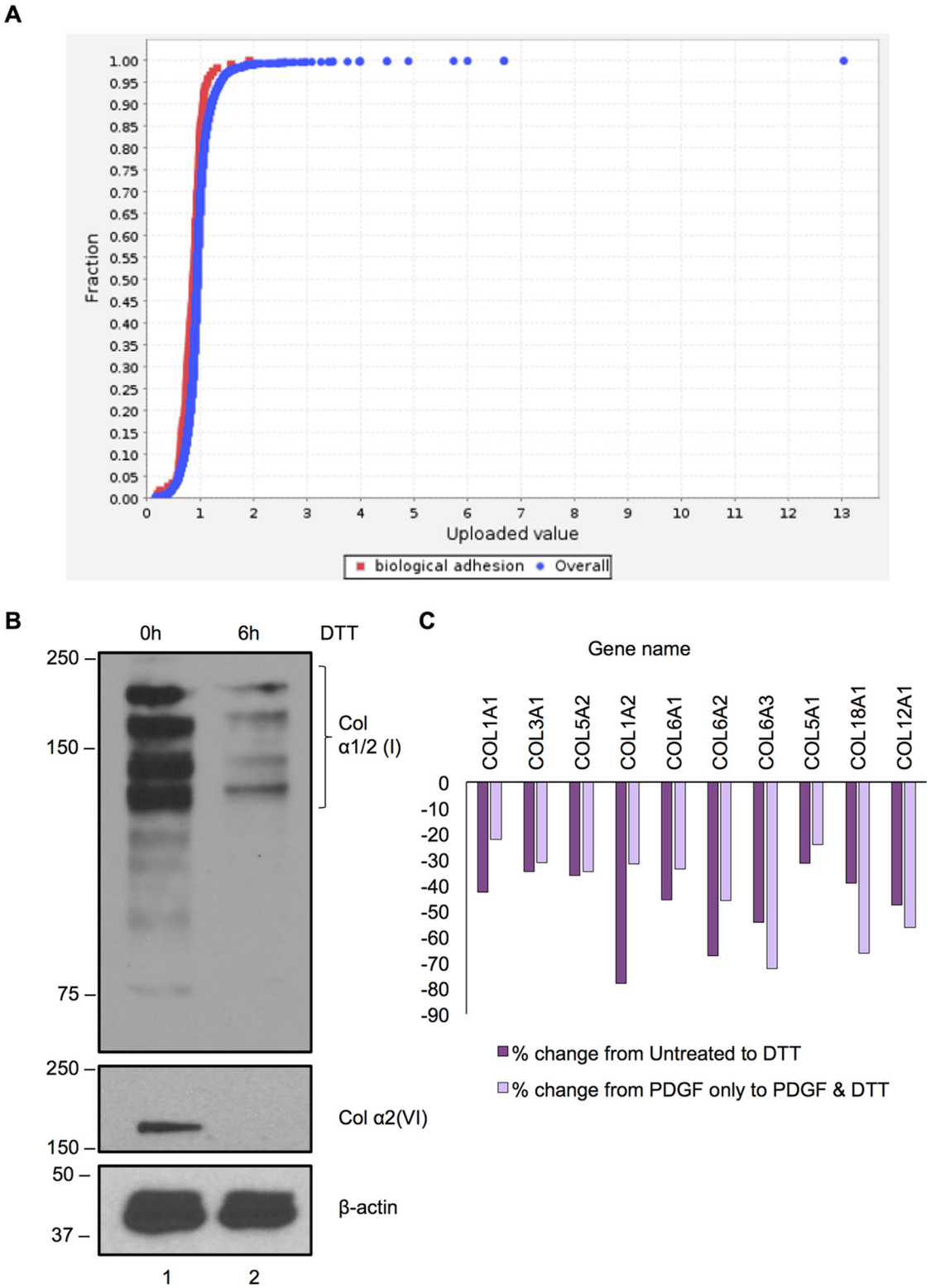

FIG. 8. **Collagens are depleted in BJ fibroblasts exposed to DTT as determined by SWATH MS.** *A*, The PANTHER Enrichment Test (released 2017-04-13) was used with PANTHER version 13.1 (released 2018-08-09) and PANTHER Go-Slim biological process annotation data set. The Bonferroni correction for multiple testing was used for significance values. Biological adhesion was significantly enriched with *p* value of 2.33×10^{-4}. *B*, Lysates from BJ fibroblasts treated for 6 h with DTT or left untreated were analyzed by 10% SDS-PAGE and immunoblotted for collagen 1 chains, collagen α2(VI), or β-actin. *C*, Percentage change in collagen proteins identified by SWATH MS was compared from samples treated ± PDGF ± DTT.

TABLE I

Coverage information for collagen proteins identified as changing negatively in response to DTT. The percentage coverage for collagen proteins with fold change (FC) greater than 1.5 and FDR adjusted p value less than 0.05 was calculated from peptide matches. Identified peptides used for coverage determination were quantified in all data sets, whether treated or otherwise. Data ranked by percentage coverage

Accession number	Gene name	No. of peptide matches	Percentage coverage (%)	DTT to untreated		PDGFDTT to PDGF only	
				FC	p-adjusted	FC	p-adjusted
CO1A1_HUMAN	COL1A1	32	32	0.57	2.25E-03	0.68	2.25E-03
CO1A2_HUMAN	COL1A2	30	31	0.22	1.25E-06	0.28	1.25E-06
CO6A3_HUMAN	COL6A3	63	20	0.46	7.05E-08	0.44	7.05E-08
COCA1_HUMAN	COL12A1	44	18	0.52	5.94E-10	0.66	5.94E-10
CO3A1_HUMAN	COL3A1	14	14	0.65	1.72E-02	0.78	1.72E-02
CO6A2_HUMAN	COL6A2	15	14	0.33	9.38E-07	0.33	9.38E-07
CO6A1_HUMAN	COL6A1	13	12	0.54	1.20E-03	0.65	1.20E-03
COIA1_HUMAN	COL18A1	7	5	0.61	4.08E-04	0.54	4.08E-04
CO5A2_HUMAN	COL5A2	4	4	0.64	5.23E-03	0.76	5.23E-03

identified in the data sets, 3 met the threshold of 2-fold change. However, a further 6 collagen proteins had a fold change of more than 1.5 (or less than 0.67) with very low FDR adjusted *p* values suggesting high levels of significance. These identifications were also made from a substantial number of peptide matches suggesting a high level of confidence (supplemental Fig. S5; Table I). The relative decrease in the detection of collagen proteins is unlikely to be explained by changes in peptide mass (*e.g.* hydroxylation at proline residues) because this is internally controlled for in the DIA reference peptide database. Decreased expression of collagen after reductive stress was confirmed by immunoblotting lysates from cells, independently treated ± DTT, for collagen 1 chains and collagen α2 (VI), with β-actin used as a loading/transfer control (Fig. 8*B*). The amount of both mature and immature collagen 1 proteins was diminished by exposure of cells to DTT. Consistent with previous observations, a comparison of the percentage decrease in relative collagen amounts with and without PDGF showed that in most, but not all, cases the response was less when PDGF was added to the treatments (Fig. 8*C*).

The stringent cutoff threshold used in the analysis has highlighted a robust set of key protein targets for future mechanistic studies of the molecular targets of reductants. The quantitative changes observed in our DIA data set cannot be accounted for simply by DTT-induced changes to the mass of the peptides analyzed (*e.g.* at cys residues), because there were no cys-containing peptides present in untreated cell lysates that were absent from reductant-exposed cell lysates; and because no differences were seen in the abundance of the majority of disulfide-containing proteins. Additionally, the relative levels of some ECM proteins, such as fibronectin and laminin, were not substantially decreased, further demonstrating that global translational attenuation in response to ER stress cannot account for the change seen in collagen abundance (Fig. 8). Taken together, our data show that a subset of collagens in fibroblasts are sensitive to a reductive environment, raising the prospect that the ECM can be selectively targeted and manipulated by redox-based chemical approaches.

DISCUSSION

Our DIA data shows that the skin fibroblast proteome is surprisingly robust when the cells experience a chronic reductive stress, with a limited set of proteins decreasing in relative quantity. The induction of ER stress by DTT and other chemical agents classically results in recruitment of the BiP protein to exposed hydrophobic domains of unfolded ER proteins, releasing BiP from ER sensors such as Ire1α to facilitate the activation of XBP1 and selective induction of ER stress responsive gene transcription (5). However, the ER stress response is both cell type and stressor specific and is under temporal control (35). In addition to gene transcription, translational regulation, microRNAs and degradative pathways can all alter the proteome profile (36). A study by Cheng *et al.* (37) showed that HeLa cells exposed to DTT experienced both a transcriptional (mRNA) and translational (protein) up-regulation of ER stress responsive proteins, using LC-MS/MS and mathematical modeling. In contrast, we show that a skin fibroblast cell type maintains a relatively stable proteome after long term (6 h DTT induced) ER/redox stress. In support of our data, Murray *et al.* have shown that lung fibroblast cells and HeLa cells have very different transcriptional responses to a variety of stressors and downregulate the transcription of some collagen and ECM proteins in response to ER stress (38). Cancer derived cell lines, such as HeLa, frequently heighten the expression of ER chaperones to provide a selective survival advantage, and may therefore be more sensitive to the induction of ER stress by chemical reagents.

A key question arising from our study is why some collagens appear particularly sensitive to reductive stress whereas other plasma membrane and disulfide-containing proteins are unaffected (Figs. 3 and 8). One possibility is PDGFR pathway-driven remodeling. Collagens and other ECM molecules can bind to and sequester PDGF at the cell surface (39). If so, sustained PDGFR pathway signaling, driven by a reductant, would trigger a feedback mechanism to decrease the level of collagens to alleviate PDGF signaling and restore cellular homeostasis. Consistent with this hypothesis, we found, from the proteomic analysis, that two peptidases involved in the

degradation of the ECM (TIMP1 and TIMP3) are oppositely regulated in PDGF-stimulated cells exposed to DTT (Fig. 3) and are candidates for restructuring the ECM of redox-challenged fibroblasts, modulating the apoptosis *versus* cell survival outcome. Collagens are likely to be more sensitive to redox stress than other proteins because they are subjected to intensive intracellular quality control, requiring disulfide bonds, glycosylation, propeptide processing, specialist packaging and export from the ER (through TANGO/cTAGE COPII exit sites), exocytosis and extracellular fibril formation, in addition to the hydroxylation of proline and lysine residues by prolyl hydroxylase and lysyl oxidase (LOX) respectively (2). It was noteworthy that in our study, LOX was one of the 41 proteins that significantly decreased in the presence of DTT, suggesting that extracellular collagen assembly becomes limiting, resulting in the degradation of incompletely processed forms. This idea is supported by the Western blotting data (Fig. 8*B*) showing that with DTT treatment, the levels of collagen α1(I) and α2(I) decline, without the accumulation of intermediate forms at steady-state. Overall, the data presented in this paper show that matrix remodeling and collagen deposition are under redox-responsive control.

Another key question is how DTT stimulates the phosphorylation of Akt in the absence of PDGF (Figs. 5 and 6). One possibility is that DTT partially reduces the PDGF receptor (or Raf/MEK kinases upstream of Akt) and causes a conformational change that triggers downstream signaling in the absence of growth factors. However, to date we have found no evidence of PDGFR autophosphorylation in cells subjected to DTT. A second possibility is that the reductive capacity of DTT modulates an Akt regulatory phosphatase such as PHLPP (40), shifting the equilibrium of Akt to the phosphorylated state. It has been shown that the PDGFR pathway phosphatase SHP2 is regulated by reversible oxidation of a thiolate at the active site (41) and that PTP1B is also modulated in this way (42). The PH domain of PHLPP has several cysteine residues that are potentially redox modifiable, and it will be interesting to determine whether this phosphatase becomes post-translationally altered after exposure to reductants. Future work to dissect the ERK/Akt signaling pathways in detail will be required to pinpoint the precise mechanism(s) of reductant induced phosphorylation and dephosphorylation. A key study published while this manuscript was in revision has proposed that ERK and Akt regulate an early step in the ER export of a subset of secreted proteins (43). Subramanian *et al.* have shown that ERK and Akt are differentially phosphorylated in HeLa and fibroblast cells upon ER exit of secretory cargoes (VSV-G and PC-1 proteins), highlighting the physiological relevance of our study to proteostasis.

The experiments demonstrating that DTT and other physiological reductants such as taurine (Fig. 7) ultimately result in dephosphorylation of MAPK suggest that a MAPK phosphatase such as mitogen-activated protein kinase phosphatase 1 or 3 (MKP-1/3) must be recruited to ERK1/2 during chronic reductive stress, but the mechanism is unknown. It is notable that Shc interacts directly with ERK to prevent ERK activation (44). The Shc interaction loop contacting ERK contains a cysteine, thus it will be informative to determine whether this interaction is also redox-regulated and diminished by reductants. Ultimately, it will be important to assess the dynamic phosphoproteome of fibroblasts exposed to reductive stress, to determine which phosphatase or phosphatases dephosphorylate ERK1/2, and to establish whether phosphatase inhibition makes cells susceptible to oxidative stress-induced aging.

In a study on lipopolysaccharide-induced cardiac dysfunction in mice, Dong *et al.* showed that chronic Akt activation can protect against apoptosis and ER stress (45). Indeed, signaling through the MAPK/Akt pathway seen in our experiments did not result in cell death or senescence under short-term conditions of reductive stress (Fig. 6 and supplemental Fig. S3), despite the activation of an ER stress response through XBP1 (Fig. 1). Instead, we found that acute DTT treatment significantly promoted the migration of PDGF-stimulated fibroblasts into a scratch-wound (supplemental Fig. S4). Although a pleiotropic bulk reductant like DTT is not a suitable drug candidate, our data clearly show that targeted and specific redox active compounds have potential for application in wound healing, where two major factors are migration of cells into the wound to achieve wound closure (driven by the PDGFR signaling pathway) and the deposition of high quality ECM to avoid scarring and fibrosis (controlled in part by collagen remodeling). Our data is also supported by a skin aging study that showed that a subset of the secretory proteins that we have identified as sensitive to reductive stress are dysregulated in aged dermal fibroblast skin cell secretomes, including collagen I alpha chains, endosialin, carboxypeptidases and fibrillins (46). Further, of the top 20 proteins that we have uncovered as downregulated in fibroblasts upon exposure to reductants, 15 are dysregulated with age in a multidecade and ethnicity study of the dermis (47), demonstrating that our reductive stress approach has the capacity to reveal genes, proteins and pathways associated with biological processes *in vivo*.

An important finding from this study is that no significant changes to the amounts of downstream ER stress target proteins were identified by DIA analysis (Figs. 3 and 4), including the ER chaperones BiP and gp96 (Fig. 5*B*). The fold changes seen for these chaperones at steady-state were 0.99 and 0.97 respectively when comparing DTT to untreated samples (Supplementary excel data). These results are consistent with the findings of the Molinari group (48) who showed that DTT does not recapitulate the ER stress response that is induced by physiologically misfolding proteins. Our data show that DTT, despite being a general reductant, selectively influences redox signaling and indirectly results in longer-term changes to the ECM. It was notable from our data set that the amount of the ER/Golgi resident chloride channel CLCC1 was depleted nearly 3-fold (fold change 0.35, FDR adjusted *p* value 0.00041) by DTT (Figs. 3 and 4). Jia *et al.* have shown

that dysfunction and disruption of CLCC1 causes an ER stress response, thus an intriguing possibility is that the induction of ER stress by DTT is indirectly caused by a loss of chloride homeostasis (49). One well-known consequence of long-term DTT exposure is that cells become less adherent to tissue culture plastics. Our data explain this phenomenon—loss of protein-protein and protein-substrate interactions—as a result of selective loss of ECM components.

Our wide-ranging findings are also relevant to skin disorders such as scleroderma, an immune-mediated condition characterized by massive fibrosis of the skin and other organs, which results in death through end-stage organ failure. Patients with scleroderma often generate excessive reactive oxygen species (50) and can be treated with imatinib mesylate (Gleevec), a tyrosine kinase inhibitor that inhibits TGFβ and PDGF signaling pathways. Imatinib prevents the development of inflammation-driven experimental fibrosis (51). The potential for small molecule reductants to counter free radical generation in scleroderma merits further investigation, to evaluate whether the potentially protective effects of the redox signaling response outweigh the negative effects associated with ER and mitochondrial stress. It will be important to understand whether myofibroblasts from scar tissue respond in the same way to reductants as fibroblasts from other sites such as facial tissue, which derive from the neural crest. In particular, the decreased expression of Wnt5a that occurs in BJ fibroblasts exposed to DTT (Figs. 3 and 4) also deserves attention: the Wnt/βcatenin pathway is required for hair follicle growth and can be targeted to reprogram ECM deposition in adult dermal fibroblasts (52), suggesting that bespoke redox reagents could be developed to influence ECM deposition in different fibroblast subpopulations. Taken together, the use of DIA technology has highlighted a small but exciting set of novel redox-regulated targets for further evaluation in skin tissue models.

Acknowledgments—We thank Nick Morrice (SCIEX), Robert Graham (Stoller Biomarker Discovery Center, University of Manchester, UK) and the Hubbard laboratory (University of Manchester, UK) for advice on DIA/SWATH data analysis; Tim Hawkins, Colin Jahoda and Melissa Jackson (Durham University, UK) for assistance with microscopy; Kirsty Goncalves (Durham University, UK) for assistance with antibodies; and Elena Lurieluke, Rosemarie Osborne and Jim Thompson (P&G) for supportive discussions.

DATA AVAILABILITY

The mass spectrometry data have been deposited to the ProteomeXchange Consortium via the PRIDE (20) partner repository with the data set identifier PXD010747 and can be accessed at http://proteomecentral.proteomexchange.org/cgi/GetDataset.

[S] This article contains supplemental Figures. The authors declare that they have no conflicts of interest with the contents of this article.

** To whom correspondence should be addressed: Department of Biosciences, Durham University, Stockton Road, Durham, DH1 3LE, UK. Tel.: +44 (0)191 334 1259; Fax: +44 (0)191 334 1201; E-mail: adam.benham@durham.ac.uk.

Author contributions: N.A.C., M.J.F., and A.M.B. designed research; N.A.C. and S.B. performed research; N.A.C., A.P.B., A.M., M.J.F., and A.M.B. analyzed data; N.A.C. and A.M.B. wrote the paper; A.P.B. contributed new reagents/analytic tools; A.P.B. deposition and curation of data in liaison with PRIDE.

REFERENCES

1. Sorrell, J. M., and Caplan, A. I. (2004) Fibroblast heterogeneity: more than skin deep. *J. Cell Sci.* **117,** 667–675
2. Malhotra, V., and Erlmann, P. (2015) The pathway of collagen secretion. *Annu. Rev. Cell Dev. Biol.* **31,** 109–124
3. Shoulders, M. D., and Raines, R. T. (2009) Collagen Structure and Stability. *Annu. Rev. Biochem.* **78,** 929–958
4. Marutani, T., Yamamoto, A., Nagai, N., Kubota, H., and Nagata, K. (2004) Accumulation of type IV collagen in dilated ER leads to apoptosis in Hsp47-knockout mouse embryos via induction of CHOP. *J. Cell Sci.* **117,** 5913–5922
5. Harding, H. P., Calfon, M., Urano, F., Novoa, I., and Ron, D. (2002) Transcriptional and translational control in the mammalian unfolded protein response. *Annu. Rev. Cell Dev. Biol.* **18,** 575–599
6. Urano, F., Wang, X., Bertolotti, A., Zhang, Y., Chung, P., Harding, H. P., and Ron, D. (2000) Coupling of stress in the ER to activation of JNK protein kinases by transmembrane protein kinase IRE1. *Science.* **287,** 664–666
7. Nishitoh, H., Matsuzawa, A., Tobiume, K., Saegusa, K., Takeda, K., Inoue, K., Hori, S., Kakizuka, A., and Ichijo, H. (2002) ASK1 is essential for endoplasmic reticulum stress-induced neuronal cell death triggered by expanded polyglutamine repeats. *Genes Dev.* **16,** 1345–1355
8. Jamsa, E., Simonen, M., and Makarow, M. (1994) Selective retention of secretory proteins in the yeast endoplasmic reticulum by treatment of cells with a reducing agent. *Yeast Chichester Engl.* **10,** 355–370
9. Deuel, T. F., Silverman, N. J., and Kawahara, R. S. (1988) Platelet-derived growth factor: a multifunctional regulator of normal and abnormal cell growth. *BioFactors.* **1,** 213–217
10. Collins, B. C., Hunter, C. L., Liu, Y., Schilling, B., Rosenberger, G., Bader, S. L., Chan, D. W., Gibson, B. W., Gingras, A.-C., Held, J. M., Hirayama-Kurogi, M., Hou, G., Krisp, C., Larsen, B., Lin, L., Liu, S., Molloy, M. P., Moritz, R. L., Ohtsuki, S., Schlapbach, R., Selevsek, N., Thomas, S. N., Tzeng, S.-C., Zhang, H., and Aebersold, R. (2017) Multi-laboratory assessment of reproducibility, qualitative and quantitative performance of SWATH-mass spectrometry. *Nat. Commun.* **8,** 291
11. Purvine, S., Eppel, J.-T., Yi, E. C., and Goodlett, D. R. (2003) Shotgun collision-induced dissociation of peptides using a time of flight mass analyzer. *Proteomics.* **3,** 847–850
12. Venable, J. D., Dong, M.-Q., Wohlschlegel, J., Dillin, A., and Yates III, J.R. (2004) Automated approach for quantitative analysis of complex peptide mixtures from tandem mass spectra. *Nat. Methods.* **1,** 39
13. Plumb, R. S., Johnson, K. A., Rainville, P., Smith, B. W., Wilson, I. D., Castro-Perez, J. M., and Nicholson, J. K. (2006) UPLC/MSE; a new approach for generating molecular fragment information for biomarker structure elucidation. *Rapid Commun. Mass Spectrom.* **20,** 1989–1994
14. Gillet, L. C., Navarro, P., Tate, S., Röst, H., Selevsek, N., Reiter, L., Bonner, R., and Aebersold, R. (2012) Targeted data extraction of the MS/MS spectra generated by data-independent acquisition: a new concept for consistent and accurate proteome analysis. *Mol. Cell. Proteomics* **11,** O111.016717
15. Gao, Y., Wang, X., Sang, Z., Li, Z., Liu, F., Mao, J., Yan, D., Zhao, Y., Wang, H., Li, P., Ying, X., Zhang, X., He, K., and Wang, H. (2017) Quantitative proteomics by SWATH-MS reveals sophisticated metabolic reprogramming in hepatocellular carcinoma tissues. *Sci. Rep.* **7,** 45913
16. Martins-Marques, T., Anjo, S. I., Pereira, P., Manadas, B., and Girao, H. (2015) Interacting network of the gap junction (GJ) protein connexin43 (Cx43) is modulated by ischemia and reperfusion in the heart. *Mol. Cell. Proteomics* **14,** 3040–3055
17. Xiao, W., Duan, X., Lin, Y., Cao, Q., Li, S., Guo, Y., Gan, Y., Qi, X., Zhou, Y., Guo, L., Qin, P., Wang, Q., and Shui, W. (2018) Distinct proteome remodeling of industrial Saccharomyces cerevisiae in response to prolonged thermal stress or transient heat shock. *J. Proteome Res.* **17,** 1812–1825
18. Liu, Y., Borel, C., Li, L., Muller, T., Williams, E. G., Germain, P.-L., Buljan, M., Sajic, T., Boersema, P. J., Shao, W., Faini, M., Testa, G., Beyer, A., Antonarakis, S. E., and Aebersold, R. (2017) Systematic proteome and

proteostasis profiling in human Trisomy 21 fibroblast cells. *Nat. Commun.* **8,** 1212
19. Liang, C.-C., Park, A. Y., and Guan, J.-L. (2007) In vitro scratch assay: a convenient and inexpensive method for analysis of cell migration in vitro. *Nat. Protoc.* **2,** 329
20. Rosenberger, G., Koh, C. C., Guo, T., Röst, H. L., Kouvonen, P., Collins, B. C., Heusel, M., Liu, Y., Caron, E., Vichalkovski, A., Faini, M., Schubert, O. T., Faridi, P., Ebhardt, H. A., Matondo, M., Lam, H., Bader, S. L., Campbell, D. S., Deutsch, E. W., Moritz, R. L., Tate, S., and Aebersold, R. (2014) A repository of assays to quantify 10,000 human proteins by SWATH-MS. *Sci. Data.* **1,** 140031
21. Mi, H., Huang, X., Muruganujan, A., Tang, H., Mills, C., Kang, D., and Thomas, P. D. (2017) PANTHER version 11: expanded annotation data from Gene Ontology and Reactome pathways, and data analysis tool enhancements. *Nucleic Acids Res.* **45,** D183–D189
22. Bergsten, E., Uutela, M., Li, X., Pietras, K., Ostman, A., Heldin, C. H., Alitalo, K., and Eriksson, U. (2001) PDGF-D is a specific, protease-activated ligand for the PDGF beta-receptor. *Nat. Cell Biol.* **3,** 512–516
23. Beer, H. D., Longaker, M. T., and Werner, S. (1997) Reduced expression of PDGF and PDGF receptors during impaired wound healing. *J. Invest. Dermatol.* **109,** 132–138
24. Li, W., Fan, J., Chen, M., Guan, S., Sawcer, D., Bokoch, G. M., and Woodley, D. T. (2003) Mechanism of human dermal fibroblast migration driven by type I collagen and platelet-derived growth factor-BB. *Mol. Biol. Cell.* **15,** 294–309
25. Lemin, A. J., Saleki, K., van Lith, M., and Benham, A. M. (2007) Activation of the unfolded protein response and alternative splicing of ATF6alpha in HLA-B27 positive lymphocytes. *FEBS Lett.* **581,** 1819–1824
26. Hamanaka, R. B., Bennett, B. S., Cullinan, S. B., and Diehl, J. A. (2005) PERK and GCN2 contribute to eIF2alpha phosphorylation and cell cycle arrest after activation of the unfolded protein response pathway. *Mol. Biol. Cell.* **16,** 5493–5501
27. Hou, C.-H., Lin, F.-L., Hou, S.-M., and Liu, J.-F. (2014) Cyr61 promotes epithelial-mesenchymal transition and tumor metastasis of osteosarcoma by Raf-1/MEK/ERK/Elk-1/TWIST-1 signaling pathway. *Mol. Cancer.* **13,** 236
28. Chen, X., Ye, S., Xiao, W., Wang, W., Luo, L., and Liu, Y. (2014) ERK1/2 pathway mediates epithelial-mesenchymal transition by cross-interacting with TGFβ/Smad and Jagged/Notch signaling pathways in lens epithelial cells. *Int. J. Mol. Med.* **33,** 1664–1670
29. Chatzifrangkeskou, M., Le Dour, C., Wu, W., Morrow, J. P., Joseph, L. C., Beuvin, M., Sera, F., Homma, S., Vignier, N., Mougenot, N., Bonne, G., Lipson, K. E., Worman, H. J., and Muchir, A. (2016) ERK1/2 directly acts on CTGF/CCN2 expression to mediate myocardial fibrosis in cardiomyopathy caused by mutations in the lamin A/C gene. *Hum. Mol. Genet.* **25,** 2220–2233
30. Locatelli, S. L., Giacomini, A., Guidetti, A., Cleris, L., Mortarini, R., Anichini, A., Gianni, A. M., and Carlo-Stella, C. (2013) Perifosine and sorafenib combination induces mitochondrial cell death and antitumor effects in NOD/SCID mice with Hodgkin lymphoma cell line xenografts. *Leukemia.* **27,** 1677–1687
31. Blaisdell, R. J., and Giri, S. N. (1995) Mechanism of antifibrotic effect of taurine and niacin in the multidose bleomycin-hamster model of lung fibrosis: inhibition of lysyl oxidase and collagenase. *J. Biochem. Toxicol.* **10,** 203–210
32. Trachtman, H., Futterweit, S., and Bienkowski, R. S. (1993) Taurine Prevents Glucose-Induced Lipid Peroxidation and Increased Collagen Production in Cultured Rat Mesangial Cells. *Biochem. Biophys. Res. Commun.* **191,** 759–765
33. Nakamura, K., Inoue, S., Abiko, S., Aoki, H., and Takeo, K. (1989) Improved separation of alpha chains of collagen type I, type III, and type V by noninterrupted electrophoresis using thioglycolic acid as a negatively charged reducer. *Electrophoresis.* **10,** 29–33
34. Park, J. H., Kim, C. K., Lee, S. B., Lee, K.-H., Cho, S.-W., and Ahn, J.-Y. (2016) Akt attenuates apoptotic death through phosphorylation of H2A under hydrogen peroxide-induced oxidative stress in PC12 cells and hippocampal neurons. *Sci. Rep.* **6,** 21857
35. DuRose, J. B., Tam, A. B., Niwa, M., and Glick, B. (2006) Intrinsic capacities of molecular sensors of the unfolded protein response to sense alternate forms of endoplasmic reticulum stress. *Mol. Biol. Cell.* **17,** 3095–3107
36. Vogel, C., and Marcotte, E. M. (2012) Insights into the regulation of protein abundance from proteomic and transcriptomic analyses. *Nat. Rev. Genet.* **13,** 227
37. Cheng, Z., Teo, G., Krueger, S., Rock, T. M., Koh, H. W., Choi, H., and Vogel, C. (2016) Differential dynamics of the mammalian mRNA and protein expression response to misfolding stress. *Mol. Syst. Biol.* **12,** 855
38. Murray, J. I., Whitfield, M. L., Trinklein, N. D., Myers, R. M., Brown, P. O., and Botstein, D. (2004) Diverse and specific gene expression responses to stresses in cultured human cells. *Mol. Biol. Cell.* **15,** 2361–2374
39. Somasundaram, R., and Schuppan, D. (1996) Type I, II, III, IV, V, and VI collagens serve as extracellular ligands for the isoforms of platelet-derived growth factor (AA, BB, and AB). *J. Biol. Chem.* **271,** 26884–26891
40. Gao, T., Furnari, F., and Newton, A. C. (2005) PHLPP: a phosphatase that directly dephosphorylates Akt, promotes apoptosis, and suppresses tumor growth. *Mol. Cell.* **18,** 13–24
41. Meng, T.-C., Fukada, T., and Tonks, N. K. (2002) Reversible oxidation and inactivation of protein tyrosine phosphatases in vivo. *Mol. Cell.* **9,** 387–399
42. Dagnell, M., Frijhoff, J., Pader, I., Augsten, M., Boivin, B., Xu, J., Mandal, P. K., Tonks, N. K., Hellberg, C., Conrad, M., Arner, E. S. J., and Ostman, A. (2013) Selective activation of oxidized PTP1B by the thioredoxin system modulates. *Proc. Natl. Acad. Sci. U.S.A.* **110,** 13398–13403
43. Subramanian, A., Capalbo, A., Iyengar, N. R., Rizzo, R., di Campli, A., Di Martino, R., Lo Monte, M., Beccari, A. R., Yerudkar, A., del Vecchio, C., Glielmo, L., Turacchio, G., Pirozzi, M., Kim, S. G., Henklein, P., Cancino, J., Parashuraman, S., Diviani, D., Fanelli, F., Sallese, M., and Luini, A. (2019) Auto-regulation of secretory flux by sensing and responding to the folded cargo protein load in the endoplasmic reticulum. *Cell.* **176,** 1461–1476.e23
44. Suen, K. M., Lin, C.-C., George, R., Melo, F. A., Biggs, E. R., Ahmed, Z., Drake, M. N., Arur, S., Arold, S. T., and Ladbury, J. E. (2013) Interaction with Shc prevents aberrant Erk activation in the absence of extracellular stimuli. *Nat. Struct. Mol. Biol.* **20,** 620–627
45. Dong, M., Hu, N., Hua, Y., Xu, X., Kandadi, M. R., Guo, R., Jiang, S., Nair, S., Hu, D., and Ren, J. (2013) Chronic Akt activation attenuated lipopolysaccharide-induced cardiac dysfunction via Akt/GSK3β-dependent inhibition of apoptosis and ER stress. *Biochim. Biophys. Acta.* **1832,** 848–863
46. Waldera Lupa, D. M., Kalfalah, F., Safferling, K., Boukamp, P., Poschmann, G., Volpi, E., Götz-Rösch, C., Bernerd, F., Haag, L., Huebenthal, U., Fritsche, E., Boege, F., Grabe, N., Tigges, J., Stühler, K., and Krutmann, J. (2015) Characterization of skin aging–associated secreted proteins (SAASP) produced by dermal fibroblasts isolated from intrinsically aged human skin. *J. Invest. Dermatol.* **135,** 1954–1968
47. Kimball, A. B., Alora-Palli, M. B., Tamura, M., Mullins, L. A., Soh, C., Binder, R. L., Houston, N. A., Conley, E. D., Tung, J. Y., Annunziata, N. E., Bascom, C. C., Isfort, R. J., Jarrold, B. B., Kainkaryam, R., Rocchetta, H. L., Swift, D. D., Tiesman, J. P., Toyama, K., Xu, J., Yan, X., and Osborne, R. (2018) Age-induced and photoinduced changes in gene expression profiles in facial skin of Caucasian females across 6 decades of age. *J. Am. Acad. Dermatol.* **78,** 29-39.e7
48. Bergmann, T. J., Fregno, I., Fumagalli, F., Rinaldi, A., Bertoni, F., Boersema, P. J., Picotti, P., and Molinari, M. (2018) Chemical stresses fail to mimic the unfolded protein response resulting from luminal load with unfolded polypeptides. *J. Biol. Chem.* **293,** 5600–5612
49. Jia, Y., Jucius, T. J., Cook, S. A., and Ackerman, S. L. (2015) Loss of Clcc1 results in ER stress, misfolded protein accumulation, and neurodegeneration. *J. Neurosci.* **35,** 3001–3009
50. Murrell, D. F. (1993) A radical proposal for the pathogenesis of scleroderma. *J. Am. Acad. Dermatol.* **28,** 78–85
51. Distler, J. H. W., Jungel, A., Huber, L. C., Schulze-Horsel, U., Zwerina, J., Gay, R. E., Michel, B. A., Hauser, T., Schett, G., Gay, S., and Distler, O. (2007) Imatinib mesylate reduces production of extracellular matrix and prevents development of experimental dermal fibrosis. *Arthritis Rheum.* **56,** 311–322
52. Collins, C. A., Kretzschmar, K., and Watt, F. M. (2011) Reprogramming adult dermis to a neonatal state through epidermal activation of beta-catenin. *Development* **138,** 5189–5199